ChemComm

COMMUNICATION

View Article Online
View Journal | View Issue

Cite this: *Chem. Commun.*, 2024, **60**, 13032

Received 6th September 2024,
Accepted 10th October 2024

DOI: 10.1039/d4cc04599h

rsc.li/chemcomm

Papain functionalized Prussian blue nanozyme colloids of triple enzymatic function†

Attila Voros, Tibor G. Halmagyi, Szilard Saringer, Viktoria Hornok and Istvan Szilagyi *

Prussian blue nanozymes were surface engineered with papain enzyme to develop processable nanoparticle dispersions with antioxidant and hydrolytic activities for biocatalytic applications. Enzyme coating improved the colloidal stability of the nanozymes and the obtained papain-Prussian blue hybrid showed remarkable peroxidase (v_{max} = 8.82 × 10^{-9} M s^{-1}, K_M = 12.3 mM), superoxide dismutase (IC_{50} = 14.6 ppm) and protease-like (41.2 U L^{-1}) activities.

The field of nanozymes, artificial enzyme mimicking nanomaterials, attracts vivid research activity nowadays.[1–4] Nanozymes can replace native enzymes in a variety of (bio)catalytic reactions including decomposition of reactive oxygen species (ROS) by superoxide dismutase (SOD),[5,6] peroxidase (POD),[7,8] and catalase.[9–11] They often mimic the function of the targeted enzymes by incorporating redox active transition metals in the active centres,[12] like in the case of Prussian blue (PB), a crystalline iron(II/III) hexacyanoferrate material of proven SOD- and POD mimicking ability.[13,14] PB is widely used in nanozyme systems either alone or in conjunction with other catalytic or support materials.[13,15–17] The advantages of the latter approach, *i.e.*, composite fabrication, are multiple.[18] For instance, the colloidal features can be altered by deposition on carriers, while combining different nanozymes can yield multienzymatic activity by either additive or synergistic mechanisms.[12,19–21] Although PB-based composites have been comprehensively explored as antioxidant nanozymes for broad-spectrum ROS scavenging,[13,16] other types of enzyme-like functions (*e.g.*, hydrolytic activity) of such hybrid materials would also be beneficial in certain applications.

Protease (PRT) enzymes, catalysts for the breakdown of proteins into peptides or even to single amino acids, include papain (PPN)[22] used in many industrial applications and research in both bare and immobilized forms.[23] PPN is positively charged below its isoelectric point (IEP, at pH 8.7) and thus, can be attached to the surface of negatively charged carrier particles.[23,24] Such enzyme immobilization methods are commonly utilized for the preservation of catalytic performance under conditions where the enzyme would ordinarily lose activity.[25] In addition, surface-immobilized PPN has been proven to improve the colloidal stability of the support, *e.g.*, preventing aggregation in high ionic strength environments *via* electrosteric stabilization.[26]

Combination of POD and PRT functions is desired in applications, in which parallel enzymatic elimination of hydrogen peroxide and hydrolysis of proteins is problematic due to the PPN attack on the POD enzyme present in the same sample. Thus, the synthesis, characterization and biocatalytic activity assessment of PB-PPN hybrid systems are presented herein. The composites were obtained *via* electrostatic adsorption, which was followed by light scattering techniques to determine the optimal experimental conditions. The main goal was to design PB-PPN colloids of high dispersion stability and efficient antioxidant and hydrolytic functions.

Details of materials and measurement protocols applied are given in the ESI.† PB nanocubes were synthesized with the polyvinylpyrrolidone (PVP) templating method, as described in the ESI.†[27,28]

The PB-PPN bionanocomposite was subsequently fabricated by direct adsorption of the positively charged PPN to the negatively charged PB surface. To ascertain the optimum amount of PPN, dose-dependent size (by dynamic light scattering (DLS)) and mobility (by electrophoretic light scattering (ELS)) measurements were performed at 40 ppm PB concentration (Fig. 1). The value of the initially highly negative electrophoretic mobility of PB starts increasing at 30 mg g^{-1} (with respect to PB content) PPN dose and reaches the IEP (PPN concentration, at which overall surface charge is zero) at about 80 mg g^{-1}. Beyond this dose, surface charge increases further, reaching the adsorption saturation plateau (ASP, the PPN level, beyond which surface charge is constant) at about 250 mg g^{-1}. Similar charge inversion was observed in other colloidal systems containing oppositely charged components[29] including PPN.[24,26]

Considering the above results, the surface coverage can be estimated. Given the diameter of PB (94.5 ± 21.6 nm from TEM

MTA-SZTE Momentum Biocolloids Research Group, Department of Physical Chemistry and Materials Science, Interdisciplinary Centre of Excellence, University of Szeged, 1 Rerrich Bela ter, 6720 Szeged, Hungary.
E-mail: szistvan@chem.u-szeged.hu

† Electronic supplementary information (ESI) available: Materials; experimental methods; synthesis of PB nanocubes; PB-PPN fabrication; SOD, POD and PRT assays; TEM and DLS size distribution data; hydrodynamic radii values. See DOI: https://doi.org/10.1039/d4cc04599h

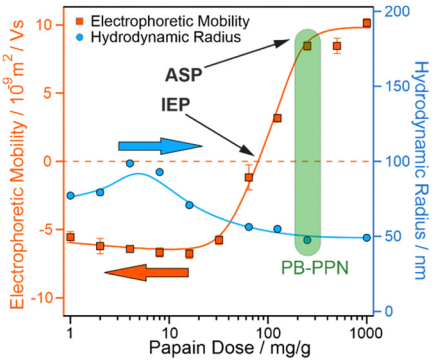

Fig. 1 Electrophoretic mobility and hydrodynamic radius values in PB-PPN systems as a function of PPN dose. A PB concentration of 40 ppm and an ionic strength of 10 mM were maintained throughout the experiment. The chosen PPN dose of 250 mg g^{-1} is marked with a green area (PB-PPN). The mg g^{-1} unit refers to mg PPN per one gram of PB.

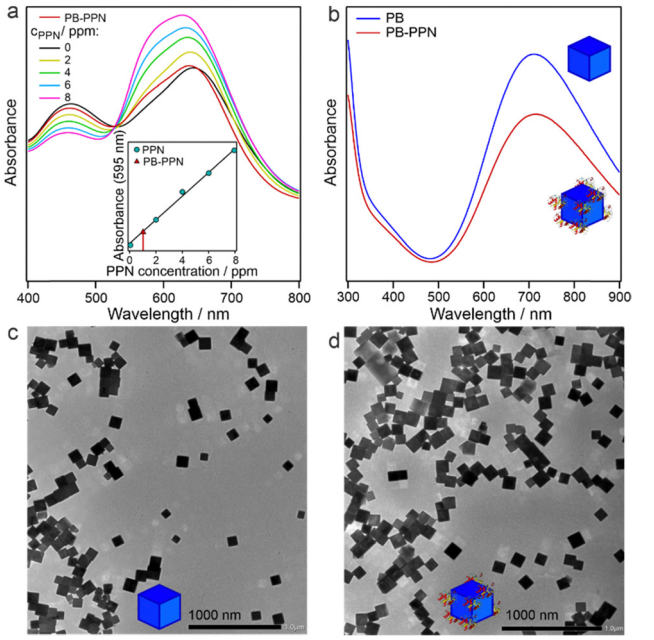

Fig. 2 UV-Vis spectra recorded in the Bradford test with PPN dilution series and 40 ppm PB-PPN (a). The inset shows the absorbances of the series and PB-PPN at 595 nm as a function of free PPN concentration. UV-Vis spectra of PB and PB-PPN at 40 ppm concentration at pH 4 (b). TEM micrographs of PB nanocubes (c) and PB-PPN particles (d).

measurements, Fig. S1a, ESI†) and PPN (7.2 nm),[30] the PPN dose for monomolecular coverage can be calculated as 26.2 mg of enzyme adsorbed on 1 gram of particles (corresponding to approximately 1000 PPN molecules per particle). Therefore, the 250 mg g^{-1} dose at the onset of ASP indicates the development of PPN multilayers on the surface. Moreover, the hydrodynamic radii (eqn S1 in the ESI†) of the particles undergo an initial increase below monolayer dosage, attributable to particle aggregation likely induced by attractive patch-charge interactions,[31] which are present at low surface coverage. Increasing the dosage leads to a decrease in particle size, as the composite is electrosterically stabilized by the protein adsorption. From these results, the 250 mg g^{-1} PPN dose was selected for further experiments (denoted as PB-PPN), since the maximum possible amount of PPN was attached to the surface and a stable dispersion was obtained.

DLS and ELS results did not yield direct information on the quantity of PPN adsorbed on the PB surface, therefore, the Bradford test was applied for such a quantification.[32,33] By comparing the UV-Vis spectra of 40 ppm PB-PPN containing 10 ppm PPN with those of a free PPN dilution series (Fig. 2a), it was found that 90% of the PPN added to the systems was adsorbed on the PB surface (Fig. 2a, inset).

This result is similar to earlier findings obtained with other support materials such as sulfate latex[24] and magnetic polymer nanoparticles.[34] A comparison of the UV-Vis spectra of 40 ppm PB and 40 ppm PB-PPN (Fig. 2b) shows no new peak appearance upon PPN adsorption, although the characteristic broad absorbance peak of PB around 720 nm is diminished due to the coverage of the nanozyme surface by PPN. This finding also indicates the successful formation of the PB-PPN hybrid.

Moreover, transmission electron micrographs of PB (Fig. 2c) and PB-PPN (Fig. 2d) show no appreciable difference between the two materials. Small-scale aggregation upon drying is observed for both systems, but the overall distribution of the primary particle size is within the experimental error with mean values of 94.5 ± 21.6 nm for PB and 102.4 ± 23.5 nm for PB-PPN (Fig. S1a and b in the ESI†). Likewise, DLS hydrodynamic size distributions of bare PB and PB-PPN are identical with a mean diameter around 95 nm (Fig. S1c, ESI†). The polydispersity index of PB and PB-PPN was 0.068 and 0.078, respectively, confirming the narrow size distribution and absence of aggregated clusters.

Resistance of PB and PB-PPN against salt- and pH-induced aggregation was tested in electrolyte solutions. The PVP-coated PB nanocubes formed stable colloids in NaCl, KCl and $CaCl_2$ even at high ionic strengths indicated by constant hydrodynamic radii in a wide range of ionic strengths (Fig. S2a, ESI†). While the charge is maximal at 30 mM NaCl concentration, the mobility decreases at higher salt levels possibly as the PB lattice incorporates some of the dissolved ions (Fig. 3a).[35] In contrast, aggregation of the PB nanoparticles occurs in $MgCl_2$ and the hydrodynamic radius data reach 600 nm at high ionic strengths (Fig. S2a, ESI†), while the critical coagulation concentration (CCC) was determined to be 714 mM (Fig. 3b). The latter value was determined in the stability ratio, measured by DLS as detailed elsewhere,[36] *versus* ionic strength plot, which showed characteristic slow (stability ratio is higher than one) and fast (stability ratio is close to unity) aggregation regions separated by the CCC. The CCC value was significantly higher than the ones reported for colloidal systems in divalent salt solutions[37,38] indicating the presence of repulsive interparticle forces of non-electrostatic origin. The importance of such forces in the stabilization mechanism is also underlined by the fact that the mobility data in $MgCl_2$ solutions remained low in the entire salt concentration regime studied (Fig. 3a), *i.e.*, the electrostatic repulsive forces were weak.

To evaluate the effect of enzyme immobilization on colloidal stability, the mobilities and radii of PB-PPN were measured in NaCl and $MgCl_2$ electrolytes. The adsorbed PPN dominates the PB-PPN surface; therefore, this material exhibits positive surface charge in both NaCl and $MgCl_2$ at low ionic strengths (Fig. 3c).

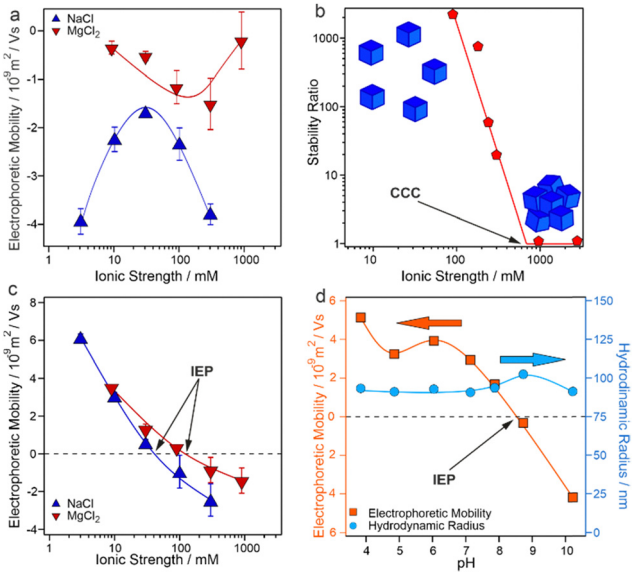

Fig. 3 Electrophoretic mobility of PB as a function of ionic strength in NaCl and $MgCl_2$ solutions (a). Stability ratio of PB *versus* ionic strength in $MgCl_2$ electrolyte (b). Electrophoretic mobility of PB-PPN as a function of the ionic strength in NaCl and $MgCl_2$ (c). The pH-dependence of electrophoretic mobility and hydrodynamic radius of PB-PPN (d). Particle concentrations were always maintained at 40 ppm.

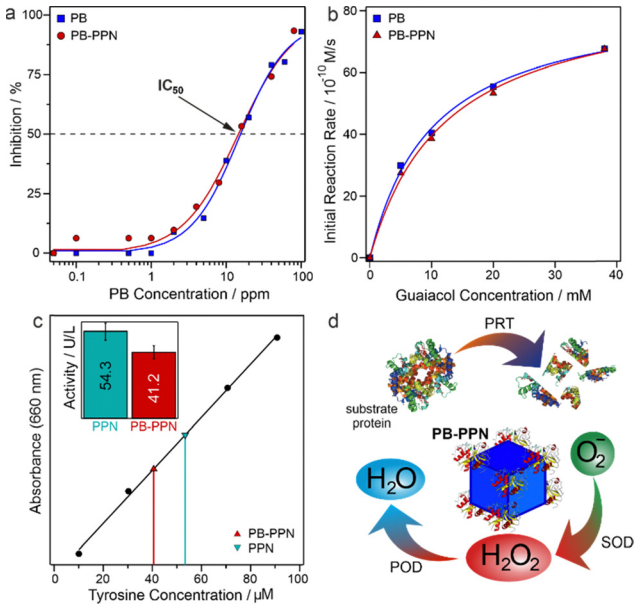

Fig. 4 SOD-like activity expressed as the inhibition of NBT-superoxide radical reaction by PB and PB-PPN (a). Experimental reaction rates (symbols) and Michaelis–Menten fit results (lines) *versus* the substrate concentration for PB and PB-PPN (b). Amount of tyrosine produced in the assay by free PPN and PB-PPN (c). Inset: PRT-like activities of PPN and PB-PPN. Nanozyme concentrations were maintained at 40 ppm in (a) and (b). PPN concentration was 10 ppm in (c). The pH value was kept at 7.0 in the SOD- and POD assays and at 7.5 in the PRT test. Schematic illustration of the multiple enzyme activity of PB-PPN (d).

Upon increasing electrolyte concentration, the mobilities decrease due to counterion condensation into the adsorbed PPN layer.[39] For NaCl, the maximum in the mobility data can be explained by the standard electrokinetic model, while for $MgCl_2$, the trend is influenced by ion specific effects at the interface.[40] Aggregation of PB-PPN is negligible in the presence of both salts, as very similar radii were determined (Fig. S2b, ESI†). These results show that PPN immobilization further improved the colloidal stability of PB and aggregation is prevented even in the divalent salt solutions. The additional stabilizing effect likely originates from steric interactions between the adsorbed PPN chains.

To ascertain whether PB-PPN also exhibits pH-independent colloidal stability, DLS and ELS measurements were performed at different pH values between 3.8 and 10.2 (Fig. 3d). The mobilities of PB-PPN are positive at acidic conditions and decrease with increasing basicity leading to zero overall charge at the IEP around pH 8.5, and to subsequent charge inversion. This IEP value is in good agreement with literature IEP data for the free enzyme (8.7).[41] The hydrodynamic radii of the particles are constant in the pH range investigated, with a slight increase around the IEP. The stability of the PB-PPN dispersions in a wide pH range implies that repulsive steric interactions dominate and electrostatic interparticle forces play a minor role. Therefore, the adsorbed PPN layer stabilizes the nanoparticles even though the charge of the enzyme itself is pH-dependent.

The ROS-scavenging activity of PB and PB-PPN was assessed in dismutation of superoxide radical ions and consumption of hydrogen peroxide (see details of the assays in the ESI†). It was observed that the unmodified nanozyme exhibits both SOD- and POD-like functions. These assays were also performed with PB-PPN as well and it was found that PB and PB-PPN possess identical SOD (Fig. 4a) and POD activity (Fig. 4b) within the experimental error, *i.e.*, the PPN adsorption did not affect the antioxidant function of PB. The IC_{50}, characteristic value of the SOD-assay indicating 50% inhibition of NBT-superoxide radical reaction (eqn S2 in the ESI†), is 15.5 ppm for PB and 14.6 ppm for PB-PPN, which indicates equal ability of the materials to dismutate superoxide radical ions. The POD-like activity was characterized by the Michaelis–Menten model (eqn S3 in the ESI†), and the maximum initial reaction rate values of PB and PB-PPN were within the error of the experimental protocol (84.7×10^{-10} M s^{-1} and 88.2×10^{-10} M s^{-1}, respectively), while the Michaelis constant of PB-PPN was only slightly higher (12.3 mM) than the one measured for PB (10.2 mM). One can conclude from these findings that PPN adsorption on the PB nanocubes did not prevent the ROS-scavenging ability of PB.

Moreover, the PRT-like function of the free PPN and the PB-PPN composite was probed with the modified Lowry assay (see details in the ESI†).[24] At identical PPN concentration (the 100 μL solutions of 100 ppm PPN and 400 ppm PB-PPN contained the same amount of the enzyme), PB-PPN exhibits 41.2 U L^{-1} activity compared to the 54.3 U L^{-1} of free PPN (Fig. 4c). This indicates 75.9% PRT activity retention upon immobilization on the PB surface. Conformational changes of native enzymes during surface adsorption often lead to a decrease in the enzymatic activity,[42,43] while enzymes were reported to be less active towards immobilized substrates.[44] Nevertheless, the present PB-PPN hybrid preserves most PRT-like activity due to the electrostatic attraction of the casein substrate to the oppositely charged particle surface with the

adsorbed PPN. Such an electrostatic interaction can play a role only in stable PB-PPN dispersions of high surface area. The remarkable PRT-like activity of PB-PPN, together with the above discussed SOD- and POD-like functions (Fig. 4d), gives further promise to this multifunctional composite in future applications.

In conclusion, a highly stable enzyme-nanozyme hybrid consisting of PPN and PB was developed. Colloidal stability and enzyme-like activity were extensively characterized. By mixing of PB and PPN, a 90% adsorption efficiency was achieved leading to inversion of the originally negative charge of the nanocubes. The PB particles were resistant to aggregation in electrolyte solutions with the exception of $MgCl_2$, in which a CCC value was determined. Enzyme immobilization further increased the colloidal stability of the composite *via* steric repulsive interactions between the adsorbed PPN chains on the surface of the particles. While bare PB aggregated in $MgCl_2$, PB-PPN remained stable until the solubility limit of the salt. The PB-PPN exhibits pH-dependent surface charge as PPN is a weak polyelectrolyte, but the size of the composite did not change in a wide pH range owing to the steric stabilization effect. The enzymatic activity of PB-PPN was examined and compared to bare PB. It was found that SOD- and POD-like activities are unchanged upon PPN adsorption, *i.e.*, the catalytic sites of PB were not blocked by the enzyme. In addition, more than 75% of the PRT activity of PPN was retained upon PB-PPN fabrication, therefore, the composite possesses a threefold (SOD, POD and PRT) enzymatic function. These results mark an advance in the field of nanozymes as well as in the fabrication of enzyme-nanozyme hybrid materials to achieve multiple enzymatic activities. Our colloid chemistry approach allows the preparation of such hybrids in stable dispersions to avoid particle aggregation, which would lead to lower surface area, phase separation and consequently, loss of enzyme-like activity.

The support of the Hungarian Academy of Sciences *via* the Momentum program (LP2022-16/2022), the SZTE Open Access Fund (7307) and the János Bolyai Research Scholarship (V. H.) is gratefully acknowledged.

Data availability

Data including electrophoretic mobility, hydrodynamic radius, UV-Vis spectra, stability ratio, absorbance, inhibition and reaction rate are available at the server of the University of Szeged faculties at **https://www.staff.u-szeged.hu/~szistvan/ChemComm_Vorosetal**.

Conflicts of interest

There are no conflicts to declare.

Notes and references

1 L. Z. Gao, H. Wei, S. J. Dong and X. Y. Yan, *Adv. Mater.*, 2024, **36**, 2305249.
2 Z. Guo, J. Hong, N. Song and M. Liang, *Acc. Mater. Res.*, 2024, **5**, 347–357.
3 Z. H. Deng, Q. L. Xiao, H. Y. Fu, S. R. Zheng, P. J. J. Alvarez, D. Q. Zhu, Z. Y. Xu and X. L. Qu, *Chem. Commun.*, 2023, **59**, 3277–3280.
4 S. Kulandaivel, C. H. Lin and Y. C. Yeh, *Chem. Commun.*, 2022, **58**, 569–572.
5 H. Q. Zhao, R. F. Zhang, X. Y. Yan and K. L. Fan, *J. Mater. Chem. B*, 2021, **9**, 6939–6957.
6 K. X. Liu, S. J. Chen, X. X. Geng, X. Y. Pei, H. Z. Xing, X. Y. Zhang, J. Chang, W. T. Yang and X. L. Wu, *ACS Mater. Lett.*, 2024, **6**, 2434–2445.
7 D. Bera, A. Mukhopadhyay, N. Nonappa and N. Goswami, *J. Phys. Chem. Lett.*, 2023, **14**, 7299–7305.
8 X. Y. Ji, Q. Lu, X. H. Sun, L. Y. Zhao, Y. H. Zhang, J. S. Yao, X. Zhang and H. Zhao, *Langmuir*, 2023, **38**, 8077–8086.
9 A. Szerlauth, T. Madácsy, G. F. Samu, P. Bíró, M. Erdélyi, G. Varga, Z. P. Xu, J. Maléth and I. Szilágyi, *Chem. Commun.*, 2024, **60**, 1325–1328.
10 Y. Y. Mao, F. M. Jia, T. Y. Jing, T. T. Li, H. M. Jia and W. W. He, *ACS Sustainable Chem. Eng.*, 2021, **9**, 569–579.
11 A. Martínez-Camarena, M. Merino, A. V. Sánchez-Sánchez, S. Blasco, J. M. Llinares, J. L. Mullor and E. García-España, *Chem. Commun.*, 2022, **58**, 5021–5024.
12 H. J. Pan, X. X. Miao, J. J. Deng, C. Z. Pan, X. G. Cheng and X. L. Wang, *ACS Appl. Mater. Interfaces*, 2023, **15**, 4935–4946.
13 N. B. Alsharif, G. F. Samu, S. Sáringer, S. Muráth and I. Szilagyi, *J. Mol. Liq.*, 2020, **309**, 113066.
14 X. Y. Ma, T. Y. Zhang, X. J. Wang, T. T. Zhang, R. Y. Zhang, Z. H. Xu, M. Z. Ma, Y. Ma and F. Shi, *ACS Appl. Nano Mater.*, 2023, **6**, 22568–22593.
15 J. Estelrich and M. A. Busquets, *Int. J. Mol. Sci.*, 2021, **22**, 5993.
16 C. Q. Chen, H. T. Wu, Q. H. Li, M. H. Liu, F. Yin, M. M. Wu, X. L. Wei, H. Wang, Z. B. Zha and F. Wang, *Biomater. Sci.*, 2023, **11**, 2348–2358.
17 Y. Zhang, X. Yuan, X. Y. Guo, H. Xu, D. X. Zhang, Z. Y. Wu and J. Zhang, *Small*, 2024, **20**, 2306961.
18 T. G. Halmagyi, L. Noureen, A. Szerlauth and I. Szilágyi, *Dalton Trans.*, 2024, **53**, 14132–14138.
19 Y. J. Jiang, Z. B. Chen, N. Sui and Z. L. Zhu, *J. Am. Chem. Soc.*, 2024, **146**, 7565–7574.
20 P. H. Ling, S. Cheng, N. Chen, C. H. Qian and F. Gao, *ACS Appl. Mater. Interfaces*, 2020, **12**, 17185–17192.
21 J. Razlivina, A. Dmitrenko and V. Vinogradov, *J. Phys. Chem. Lett.*, 2024, **15**, 5804–5813.
22 J. Drenth, J. N. Jansonius, R. Koekoek, H. M. Swen and B. G. Wolthers, *Nature*, 1968, **218**, 929–932.
23 J. Fernandez-Lucas, D. Castaneda and D. Hormigo, *Trends Food Sci. Technol.*, 2017, **68**, 91–101.
24 S. Sáringer, T. Valtner, Á. Varga, J. Maléth and I. Szilagyi, *J. Mater. Chem. B*, 2022, **10**, 2523–2533.
25 T. Jesionowski, J. Zdarta and B. Krajewska, *Adsorption*, 2014, **20**, 801–821.
26 S. Saringer, R. A. Akula, A. Szerlauth and I. Szilagyi, *J. Phys. Chem. B*, 2019, **123**, 9984–9991.
27 S. L. Wang, H. Yan, Y. L. Wang, N. Wang, Y. L. Lin and M. Li, *Microchim. Acta*, 2019, **186**, 738.
28 Z. G. Qin, B. Chen, Y. Mao, C. Shi, Y. Li, X. Huang, F. Yang and N. Gu, *ACS Appl. Mater. Interfaces*, 2020, **12**, 57382–57390.
29 M. Itatani, G. Holló, D. Zámbó, H. Nakanishi, A. Deák and I. Lagzi, *J. Phys. Chem. Lett.*, 2023, **14**, 9003–9010.
30 N. Zou and J. Plank, *J. Phys. Chem. Solids*, 2012, **73**, 1127–1130.
31 I. Szilagyi, G. Trefalt, A. Tiraferri, P. Maroni and M. Borkovec, *Soft Matter*, 2014, **10**, 2479–2502.
32 T. Zor and Z. Seliger, *Anal. Biochem.*, 1996, **236**, 302–308.
33 M. M. Bradford, *Anal. Biochem.*, 1976, **72**, 248–254.
34 P. Alpay and D. A. Uygun, *J. Mol. Catal. B: Enzym.*, 2015, **111**, 56–63.
35 X. W. He, L. D. Tian, M. T. Qiao, J. Z. Zhang, W. C. Geng and Q. Y. Zhang, *J. Mater. Chem. A*, 2019, **7**, 11478–11486.
36 G. Trefalt, I. Szilagyi, T. Oncsik, A. Sadeghpour and M. Borkovec, *Chimia*, 2013, **67**, 772–776.
37 Y. C. Chang, Z. C. Jin, K. Li, J. J. Zhou, W. Yim, J. S. Yeung, Y. Cheng, M. Retout, M. N. Creyer, P. Fajtova, T. Y. He, X. Chen, A. J. O'Donoghue and J. V. Jokerst, *Chem. Sci.*, 2023, **14**, 2659–2668.
38 G. Trefalt, I. Szilagyi and M. Borkovec, *Colloid Polym. Sci.*, 2020, **298**, 961–967.
39 M. Borkovec, G. J. M. Koper and C. Piguet, *Curr. Opin. Colloid Interface Sci.*, 2006, **11**, 280–289.
40 M. Borkovec, S. H. Behrens and M. Semmler, *Langmuir*, 2000, **16**, 5209–5212.
41 B. Sahoo, S. K. Sahu, D. Bhattacharya, D. Dhara and P. Pramanik, *Colloids Surf., B*, 2013, **101**, 280–289.
42 R. C. Rodrigues, C. Ortiz, A. Berenguer-Murcia, R. Torres and R. Fernandez-Lafuente, *Chem. Soc. Rev.*, 2013, **42**, 6290–6307.
43 C. Mateo, J. M. Palomo, G. Fernandez-Lorente, J. M. Guisan and R. Fernandez-Lafuente, *Enzyme Microb. Technol.*, 2007, **40**, 1451–1463.
44 Z. C. Jin, N. Dridi, G. Palui, V. Palomo, J. V. Jokerst, P. E. Dawson, Q. X. A. Sang and H. Mattoussi, *J. Am. Chem. Soc.*, 2023, **145**, 4570–4582.